Heliyon 10 (2024) e30263

Contents lists available at ScienceDirect

Heliyon

journal homepage: www.cell.com/heliyon

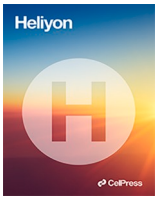

Research article

Mass scale synthesis of graphene nanosheets using waste cardboard for application in perovskite solar cells and supercapacitors

Kuldeep K. Garg [a,b,1], Sandeep Pandey [c,d,1], Mayank Pathak [e], Chetan Prakash Sharma [f], Amit Kumar [a,b], Lata Pandey [e], Christopher J. Arnusch [f], Nanda Gopal Sahoo [e], S.K. Dhawan [a], Man-Jong Lee [c,d,**], Rajiv K. Singh [a,*]

[a] *Photovoltaic Metrology Section, Advanced Materials and Devices Metrology Division, CSIR- National Physical Laboratory, Dr. K.S. Krishnan Marg, New Delhi, 110012, India*
[b] *Academy of Scientific and Innovative Research (AcSIR), Ghaziabad, Uttar Pradesh, 201002, India*
[c] *Department of Chemistry, Konkuk University, Seoul, 05029, Republic of Korea*
[d] *Advanced Crystal Material/Device Research Center, Konkuk University, Seoul, 05029, Republic of Korea*
[e] *PRS Nanoscience and Nanotechnology Centre, Department of Chemistry, D.S.B. Campus, Kumaun University, Nainital, 263001, Uttarakhand, India*
[f] *Dept. of Desalination and Water Treatment, Zuckerberg Institute for Water Research, The Jacob Blaustein Institutes for Desert Research, Ben-Gurion University of the Negev, 8499000, Midreshet Ben Gurion, Israel*

ARTICLE INFO

Keywords:
Waste cardboard
Recycling
Graphene nanosheet
Perovskite solar cell
Supercapacitor

ABSTRACT

Advanced graphene-based materials have been proficiently incorporated into next-generation solar cells and supercapacitors because of their high electrical conductivity, large surface area, excellent charge-transport ability, and exceptional optical properties. Herein, we report the synthesis of graphene nanosheets (GNs) from waste cardboard via pyrolysis, with ethyl alcohol as the growth initiator. Additionally, we demonstrated the use of GNs in energy conversion and storage applications. Using the GN electrode in perovskite solar cells resulted in an excellent power conversion efficiency of ~10.41 % for an active area of 1 cm2, indicating an enhancement of approximately 27 % compared to conventional electrodes. Furthermore, the GNs were used as active electrode materials in supercapacitors with excellent electrochemical performance and a high gravimetric specific capacitance of 167.5 F/g at a scan rate of 2 mV/s. The developed GNs can be efficiently used for energy storage, conversion, and electrochemical sensing applications.

1. Introduction

The global increase in energy consumption necessitates the development of environmentally friendly, efficient, low-cost, and sustainable methods for electrical energy storage and conversion [1]. Although conventional energy resources must be enhanced to sustain the existing energy consumption levels, several challenges exist in achieving this purpose, including poor performance,

* Corresponding author.
** Corresponding author. Department of Chemistry, Konkuk University, Seoul, 05029, Republic of Korea.
E-mail addresses: leemtx@konkuk.ac.kr (M.-J. Lee), rajivsingh@nplindia.org (R.K. Singh).
[1] These authors contributed equally to this work.

https://doi.org/10.1016/j.heliyon.2024.e30263
Received 2 January 2024; Received in revised form 11 April 2024; Accepted 23 April 2024
Available online 26 April 2024

environmental pollution, and the annihilation of resources [2,3]. Therefore, alternative renewable energy resources, such as solar, geothermal, and hydroelectric sources and fuel cells, have been explored for application in energy conversion systems. Among the available energy alternatives, solar energy is considered a clean, sustainable solution that complements conventional forms of energy. In conjunction with energy conversion systems, supercapacitors are promising energy storage components for application in electric vehicles, microgrids, and energy harvesting systems [4,5]· Supercapacitors' excellent cycling stability and high power densities render them superior to conventional aluminium electrolytic capacitors for alternative line filtering applications [6,7]. However, the materials used for manufacturing solar cells and electrodes affect their performance (D. [8]). Therefore, advanced graphene-based materials with high electrical conductivity, large surface area, excellent charge-transport ability, and exceptional optical properties are considered promising for the development of next-generation solar cells and supercapacitor devices ([9–11,11–15]; K. [16,17]). However, the bulk production of these graphene-based materials still needs to be improved.

Bulk-scale graphene production predominantly uses top-down approaches, wherein graphite is chemically exfoliated; this approach involves harsh chemical treatments and post-processing methods to reduce structural defects [18,19]. Although bottom-up approaches, such as chemical vapour deposition, can produce high-quality graphene, they are often restricted to small-scale graphene production and are helpful only for laboratory applications [20]. Thus far, considerable efforts have been devoted to producing bulk-scale graphene from low-cost or negative-monetary-value materials using thermal treatment technologies, such as gasification, oxidation, and pyrolysis [21]. The thermochemical transformation of organic waste materials into carbon materials and volatile matter using pyrolysis under inert environmental conditions (in the presence of N_2 or Ar) has exhibited significant potential for the conversion of municipal solid waste (MSW) to value-added products; this transformation is considered a feasible solution for solid waste management ([22]; X. [23]). In addition to thermochemical processes, a rapid and cost-effective method has been reported for converting waste materials into valuable graphene flakes in less than 1 s using a short electrical pulse, termed "flash graphene"[24]. Although this technology is relatively new, bulk quantities of graphene can be efficiently prepared using inexpensive carbon sources, such as coal, tyres, biochar, and plastic waste.

MSW generated from urban areas primarily comprises organic waste, plastic, paper, cardboard, textiles, leather, rubber, glass, metals, and miscellaneous materials, containing a significant amount of carbon ([25]; Barbhuiya, Kumar, Singh, Munish K [24]). According to a World Bank report, the global waste composition includes 44 % of food and green products (biowastes) and 17 % of paper and cardboard, with a significant amount of plastic, leather, wood, glass, metals, and other materials [26]. Cardboard is a

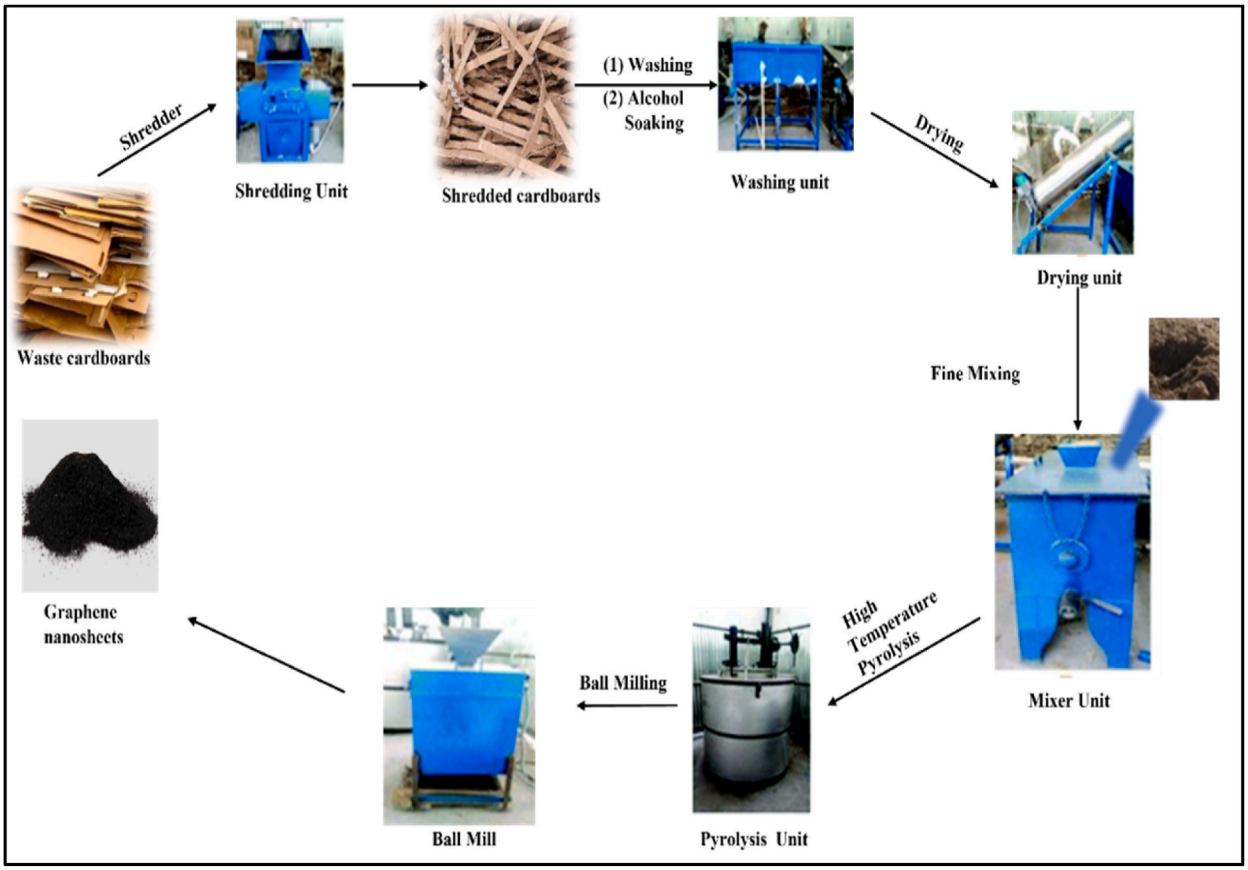

Scheme 1. Synthesis of graphene nanosheets (GNs) from waste cardboard.

commonly used packaging material, and its disposal in landfills leads to significant greenhouse gas emissions [27,28]. Therefore, transforming waste cardboard into high-quality graphene materials can facilitate waste management and yield a high-value product [28].

This study used a cost-effective pyrolysis method to prepare graphene nanosheets (GNs) from waste cardboard. The fabricated GNs were then used for energy conversion and storage applications. We successfully demonstrated the utilisation of GNs as electrode materials for perovskite solar cells (PSCs), wherein the GNs enhanced the device parameters. Additionally, we fabricated a supercapacitor device using the GNs as the active electrode material and achieved a significantly high specific capacitance with adequate cyclic stability. The study findings confirm that carbon-containing waste is a valuable source for the low-cost production of GNs, demonstrating the concept of waste-to-energy conversion using an environmentally friendly and sustainable method.

2. Material and methods

2.1. Synthesis of GNs from waste cardboard

Scheme 1 depicts the process of synthesising GNs from waste cardboard. The waste cardboard collected from a local market (about 50 kg) was shredded using a shredder, washed in 5 % aqueous ethanol solution, and dipped in 10 % aqueous ethanol overnight to prepare a slurry paste inside the washing unit.

Subsequently, the slurry paste was kneaded to yield a uniform slurry, which was crushed using a high-strength mechanical mixer inside the washing unit. This paste was dried inside the drying unit and transferred to a mixing unit, where the precursor material's dried clusters were converted into fine powder-like materials. The dried mass was then placed inside a pyrolysis reactor comprising a vertically hollow stainless-steel cylindrical feeder unit with a capacity of 0.41 m^3. Pyrolysis was performed in an N_2 atmosphere at a temperature of 700 °C with a heating rate of 10 °C/min for 70 min, which resulted in a puffy black carbon material. This material was subjected to ball milling to obtain a fine black powder, which was subsequently characterised as GNs.

2.2. Characterizations

The GNs obtained from pyrolysis were characterised using spectroscopic and imaging techniques. A confocal micro-Raman spectrometer (AIRIX, STR 500) with an excitation beam length of 532 nm was used to confirm the graphitic skeleton and the quality of the GNs. Fourier transform infrared (FT-IR) spectroscopy was performed to identify oxygen-containing functional groups within the GNs using an FT-IR spectrometer (Lambda-2, PerkinElmer). We performed X-ray photoelectron spectroscopy (XPS) using an ESCALAB 250 system (Thermo Fisher Scientific, USA) with an ultrahigh vacuum (10^{-9} bar), which was installed using an Al Kα X-ray source (beam size of 500 μm) and a monochromator to analyse the elemental composition of the powdered samples. The X-ray diffraction (XRD) analysis was performed using a Rigaku MiniFlex-II instrument with the Cu-Kα radiation of wavelength k = 1.5418 Å. The thermal stabilities of the samples were explored via thermogravimetric analysis (TGA; Q500 V20.13 Build 39 Instruments). Each sample was placed on the sample holder and heated to 1000 °C at 10 °C/min in an N_2 atmosphere (5 min purge, 90 mL/min). The surface morphologies of the prepared GNs were characterised based on field-emission scanning electron microscopy (FESEM), performed using NOVA FESEM 900 (NOVA) and JEM 2100 (JEOL, Japan) instruments. For SEM imaging, the samples were oven-dried at 60 °C for 6 h and mounted on the SEM stub using a double-sided carbon tape. Subsequently, the samples were sputter-coated with Au/Pd to collect the secondary electrons on their surfaces efficiently. High-resolution transmission electron microscopy (HRTEM) images of the GN samples were obtained using a T12 200 kV TEM instrument (FEI, TWIN Electron Optics) with an input voltage of 120 kV. Before the analysis, the powdered sample was dissolved in deionised water and sonicated for 30 min. The TEM grids were prepared by placing the 2 μL of diluted and sonicated sample solutions on a carbon-coated copper grid and evaporating them at room temperature.

2.3. Fabrication and characterisation of PSCs

After synthesising the GNs from waste cardboard, PSCs were fabricated per our previously reported methodology [29]. Herein, monolithic carbon electrodes (Solaronix) were used as the substrates, which were heated at 450 °C inside a muffle furnace for 30 min and cooled to room temperature. A methyl ammonium lead iodide ($MAPbI_3$) perovskite ink was prepared by mixing methyl ammonium iodide (MAI) and PbI_2, with a molar ratio of 1:1, in 1 ml of dimethylformamide under ambient conditions. The two devices were fabricated using two different configurations. One device (D1) was fabricated by simply depositing perovskite ink via a single-step drop-casting method, whereas the other device (D2) was fabricated using a two-step procedure. Device D2 was fabricated by drop-casting the perovskite ink and dispersing the GNs in chlorobenzene (1 mg in 2 ml). Subsequently, both devices D1 and D2 were annealed for 10 min at 70 °C and subjected to current density–voltage (J–V) measurements using a solar simulator (AM 1.5 G, class AAA, Photo Emission Tech Inc.) and a Keithley 2400 source measure system.

2.4. Preparation of electrodes and electrochemical analysis

The synthesised GNs were used as electrode materials to fabricate the supercapacitor device. The electrode was fabricated by preparing a sticky paste of GNs in a magnetic stirrer, using 10 wt% polyvinylidene fluoride in acetone, which served as a binder for the system. The prepared sticky GN paste was coated on two separate graphite sheets with 1 cm × 1 cm dimensions and dried in a vacuum oven for 24 h. The weights of non-coated and coated substrates were separately measured to calculate the mass loading of each

electrode substrate. Finally, a symmetrical supercapacitor device architecture was fabricated, wherein individually coated and dried electrodes were sandwiched by inserting a Millipore filter paper immersed in a 1 M H_3PO_4 electrolyte. The electrochemical behaviour of the device was then measured using cyclic voltammetry (CV), electrochemical impedance spectroscopy (EIS), galvanostatic charge–discharge (GCD), and cyclic stability tests. The entire testing was performed using the two-electrode system of the Metrohm Autolab electrochemical workstation.

3. Results and discussion

The physicochemical properties of the fine black powder prepared via the pyrolysis of cardboard were characterised using different spectroscopic and digital imaging techniques. Raman spectra were recorded to characterise the graphitic nature of the as-prepared powders (Fig. 1(a)). Two dominant peaks were observed in the spectra at approximately 1345.77 and 1598.38 cm^{-1}, corresponding to *D* and *G* bands, respectively. The conversion of waste cardboard into GNs during pyrolysis at high temperatures resulted in the appearance of the *D* peak, which indicated the formation of defects and the presence of sp_3 carbon atoms in the GN samples. The presence of the *G* band in the spectra of GN samples confirmed the conversion of cardboard into sp_2 hybridised carbon atoms, indicating the first-order scattering and electron transfer within the GNs. The increase in the heating rate during pyrolysis was responsible for the higher intensity of the *G* band compared with that of the *D* band in the GN sample spectra, resulting in a D-to-G band intensity ratio (ID/IG) of 0.85; this validated the presence of high domains in sp_2 carbon atoms. Furthermore, the hump-like shape at approximately 2900 cm^{-1} suggested the presence of a $D + G$ band, confirming the disorder within the GN surfaces. The FT-IR spectroscopic analysis confirmed the presence of various functional groups within the GNs (Fig. 1(b)). The recorded FT-IR spectra exhibited different peaks at approximately 3412 cm^{-1}, weak peaks at 2920 and 2862 cm^{-1}, a medium peak at 1612 cm^{-1}, a medium peak at 1410 cm^{-1}, and a sharp peak at 1058 cm^{-1}, corresponding to –OH stretching, –CH stretching, –C═C– stretching, –C═O stretching, –C–OH stretching, and –C–O stretching, respectively. The oxygen-containing groups indicated defects or impurities in the GNs, which were also observed in the Raman analysis. We performed the XRD analysis to characterise further the GN samples' graphitic nature (Fig. 1(c)). A sharp peak at $2\theta = 26.40^\circ$ and a small peak at 42.41° confirmed the graphitic characteristics of the GNs [30]. Fig. 1(d) illustrates the TGA results of the GNs, confirming the consecutive degradation of the material. The first stage of

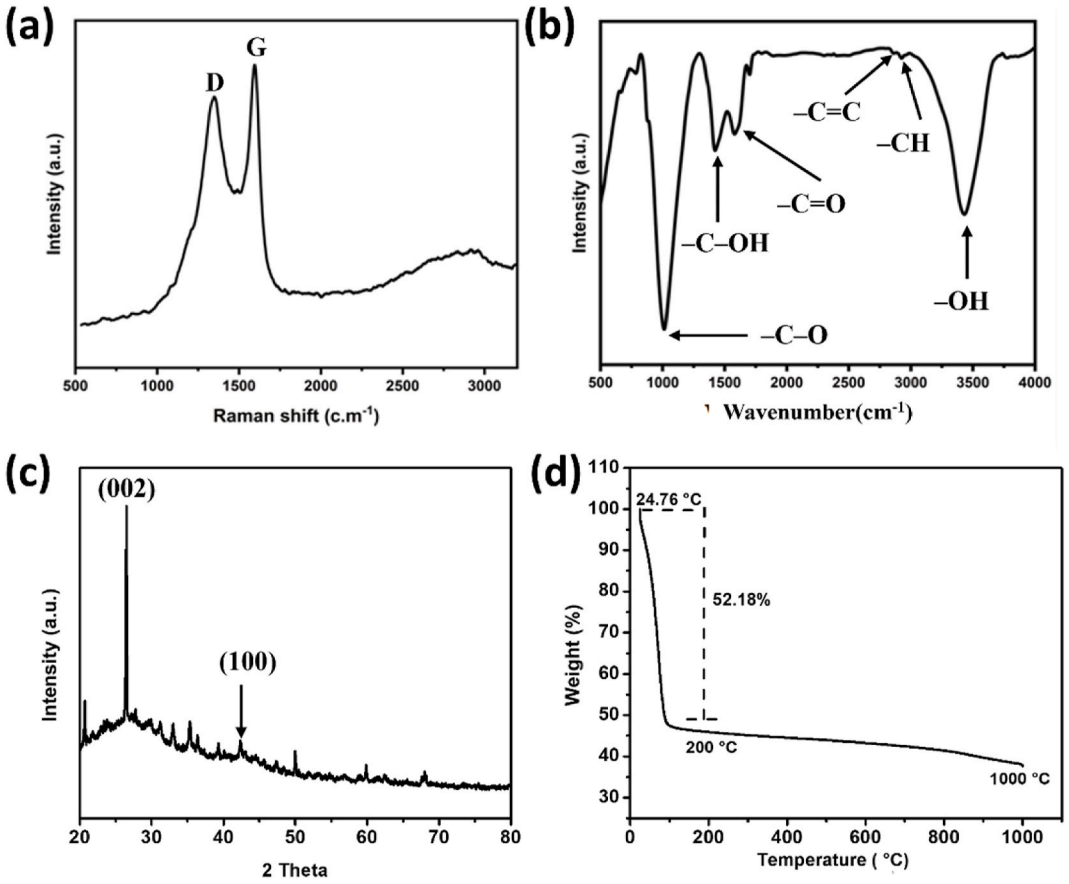

Fig. 1. (a) Raman spectra of graphene nanosheets (GNs) obtained from waste cardboard. (b) Fourier transform infrared (FT-IR) spectra of the dried GNs. (c) X-ray diffraction (XRD) analysis of GNs. (d) Thermogravimetric analysis (TGA) graph of the GNs.

degradation was identified in the range of 24.76–200 °C, indicating the presence of moisture in the GNs. The second- and third-stage degradations were observed between approximately 200 and 700 °C and 700 and 1000 °C, respectively. These were attributed to eliminating oxygen functionalities and the degradation of the carbon backbone in the GNs. An approximate weight loss of 52.18 % (approximately 100–200 °C) was caused by removing the excess water content in the structure of GNs. However, in the range of 200–1000 °C, approximately 8.15 % of the total weight loss indicated high thermal stability, confirming the pure graphitic composition of the GNs.

The atomic chemical composition of the fabricated GNs was further analysed using XPS. Fig. 2(a) depicts the wide-scan XPS spectra of the GNs, indicating two significant peaks for O 1s and C 1s at 532.78 and 284.81 eV, respectively, corresponding to carbon and oxygen as the major chemical components, respectively. However, the minimal amounts of <1 % nitrogen and iron were attributed to the impurities associated with the raw cardboard samples. In Fig. 2(b), a slight shift of C 1s peaks from 284.8 to ~284.7 eV indicates the presence of sp_2 and sp_3 hybrid carbon atoms in the GN samples [11]. The presence of >10 % carbon in the form of C═O and O–C═O confirms that the prepared GNs contain a distorted or non-uniform graphene structure, which can be attributed to the high temperature and long duration of the pyrolysis process. Additionally, the deconvoluted O 1s spectra indicate the presence of C═O, C–OH, and C–O–C bonds in the GN samples at 531.7, ~532.66, and 533.64 eV, respectively (Fig. 2(d)).

We performed HRTEM further to investigate the internal morphology and structure of the GNs. The HRTEM images indicated that the size of GNs was in the micrometre range (Fig. 3(a)). Additionally, the presence of wrinkled and rippled structures confirmed the formation of multilayered GNs, resulting in a large surface area; this renders the material suitable for fabricating electrodes of third-generation solar cells and supercapacitors, as reported previously [24]. The rippled structure of the GNs was attributed to the thermal expansion of the cardboard during pyrolysis (Fig. 3(b)) [31]. Furthermore, the surface morphology of the GN powder verified the nanometer scale of the graphene sheets.

We also observed grain boundaries and corrugated edges in the HRTEM images, which render the GN material suitable for fabricating electrodes of third-generation solar cells and supercapacitors, as reported previously [32]. The FESEM images of the GNs indicate the porous and rough surface morphologies of the synthesised GNs, which are known to endow the GNs with metallic behaviour [30]. The hill stack plot derived from the FESEM image of the GNs confirmed the surface roughness and porosity of the GNs and the presence of corrugated edges, which further validated the suitability of GNs for supercapacitor applications (Fig. 3(c)). Furthermore, the three-dimensional (3D) surface morphology observed in the FESEM images of the GNs was analysed based on the

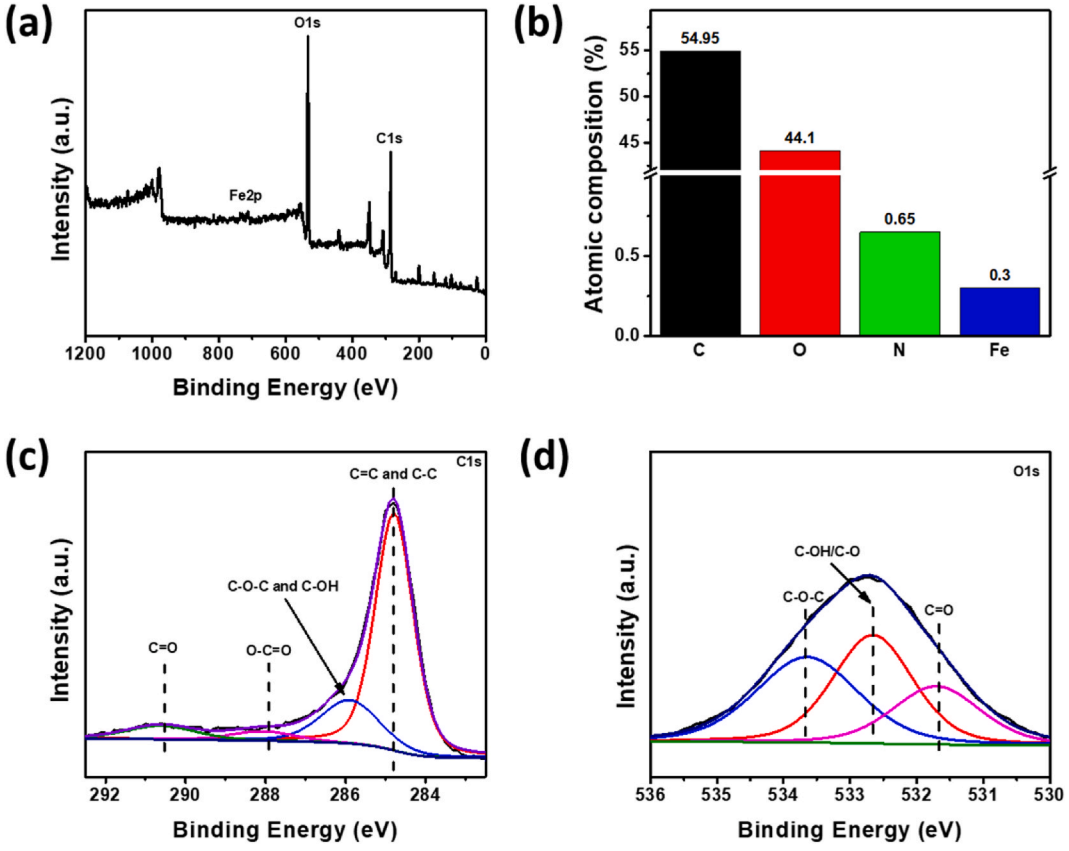

Fig. 2. (a) X-ray photoelectron spectroscopy (XPS) spectra of the fabricated graphene nanosheets (GNs). (b) Elemental composition of GNs. Deconvoluted XPS spectra: (c) C 1*s* (d) and O 1*s* peaks.

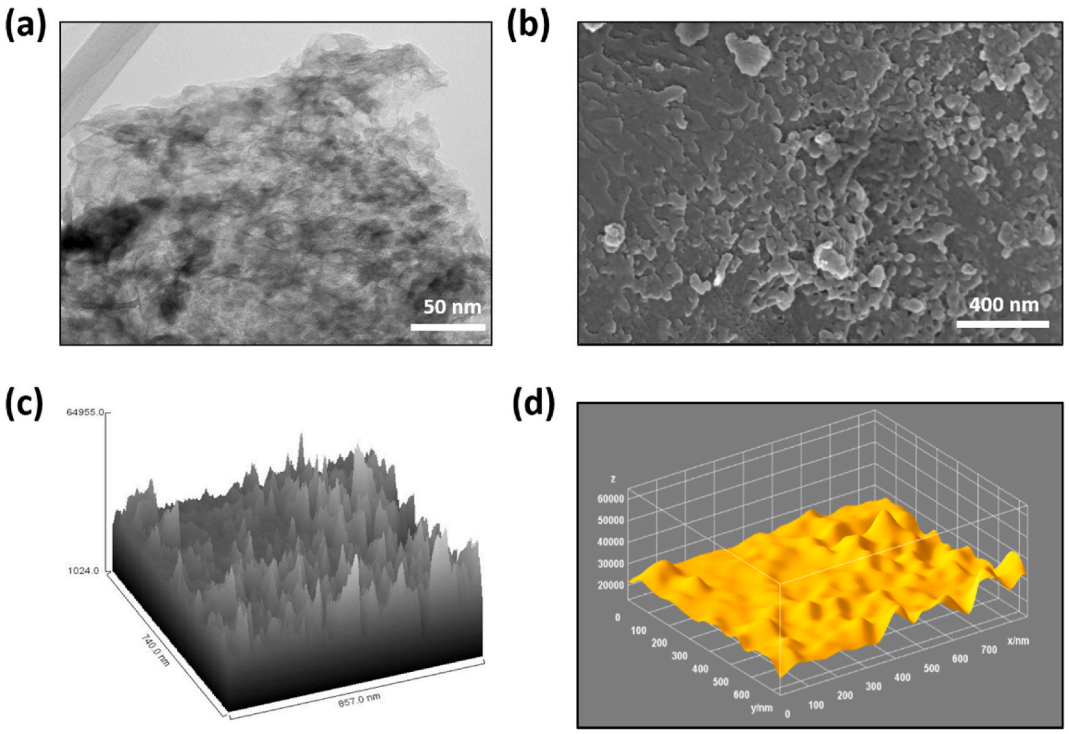

Fig. 3. (a) High-resolution transmission electron microscopy (HRTEM) images of the graphene nanosheets (GNs) obtained from waste cardboard. (b) Field-emission scanning electron microscopy (FESEM) image of the fabricated GNs. (c) Hill stack plot of the FESEM image of the GNs. (d) Three-dimensional (3D) surface morphology obtained from the FESEM image of the GNs.

topology of the GNs, which indicated the interconnected networks of the few-layer stacks of the GNs. Fig. 3(d) suggests that each stack of the GNs is well connected to the other stacks. The 3D surface morphology of the GNs further confirmed the presence of corrugated edges, which can be beneficial for supercapacitor applications [10]. Therefore, the synthesised GNs can be used as a universal material for energy conversion and storage applications.

Graphene is widely known for its rapid charge-transport ability, which helps improve photovoltaic device characteristics. Therefore, we fabricated PSCs to analyse the applicability of GNs in photoconversion applications. Incorporating GNs into the carbon electrodes of PSCs enhanced the charge transportation and reduced recombination losses. The high conductivity and large surface area of the GNs facilitated the transportation of electrons from the perovskite layer to the carbon electrode, thereby reducing the charge recombination losses. Moreover, incorporating GNs enhanced the stability and durability of PSCs by preventing carbon electrode degradation under harsh operating conditions. One of the perovskite solar cell devices (D1) was fabricated on the printed monolithic carbon electrode with the configuration of glass/FTO/TiO_2/ZrO_2/conducting carbon (Fig. 4(a)). Herein, the $MAPbI_3$ perovskite layer was deposited via the drop-casting method. The other PSC device (D2) was fabricated on the same monolithic carbon electrode by drop-casting the same $MAPbI_3$ perovskite ink, followed by the drop-casting of the dispersion of GNs in carbon black. Both devices were then annealed at 70 °C for 10 min (Scheme 2).

However, the GN-treated device D2 absorbed the perovskite ink, and a dense dispersion of GNs was added to the upper layer of the electrode. Owing to the large surface area of GNs, the GN particles failed to cross the microchannels of the porous carbon layer, thereby uniformly spreading on the carbon layer surface. Additionally, the dispersion of GNs in chlorobenzene served as a dual performer to improve the device performance by increasing the current density and V_{oc}, which was reflected in the device's power conversion efficiency (PCE). This improvement was primarily because of the smooth transportation of charges at the upper interface, which improved the device's fill factor (FF). Fig. 4(b) depicts the J–V characteristics of the untreated (D1) and treated (D2) devices, where the red and black lines represent the untreated device (reference device) and the treated device, respectively. Table 1 lists the comparative parameters of the two devices.

As indicated in Table 1, the short-circuit current (J_{sc}), Voc, and FF of the GN-treated device (D2) improved compared with those of the untreated device (D1). Consequently, the overall PCE increased from 13.98 to 15.80 % for a large active area of 1 cm^2. This increase in the PCE validates that incorporating GNs decelerates the recombination process and improves the interface properties between the carbon electrode and perovskite layer. Further, we also investigated the photocurrent (J_{ph}), which can be estimated by subtracting the dark current ($J_{D)}$ from the light current (J_L), i.e. $J_{ph} = J_L$-$J_{D,}$ and simultaneously plotted with the effective applied bias voltage, i.e. V_{eff} = V_o-V, where V_o is referred to the compensation voltage at which light current is equal to the dark current, i.e. $J_L = J_{D.}$ Fig. 4 (c) showed an apparent change in the effective bias voltage in the control and graphene-added device. Jph is linearly proportional to Vo -V up to 0.3 V for untreated devices, as shown in Fig. 4(c). By comparing the J_{ph} vs V_o -V graph of untreated and treated devices, it has

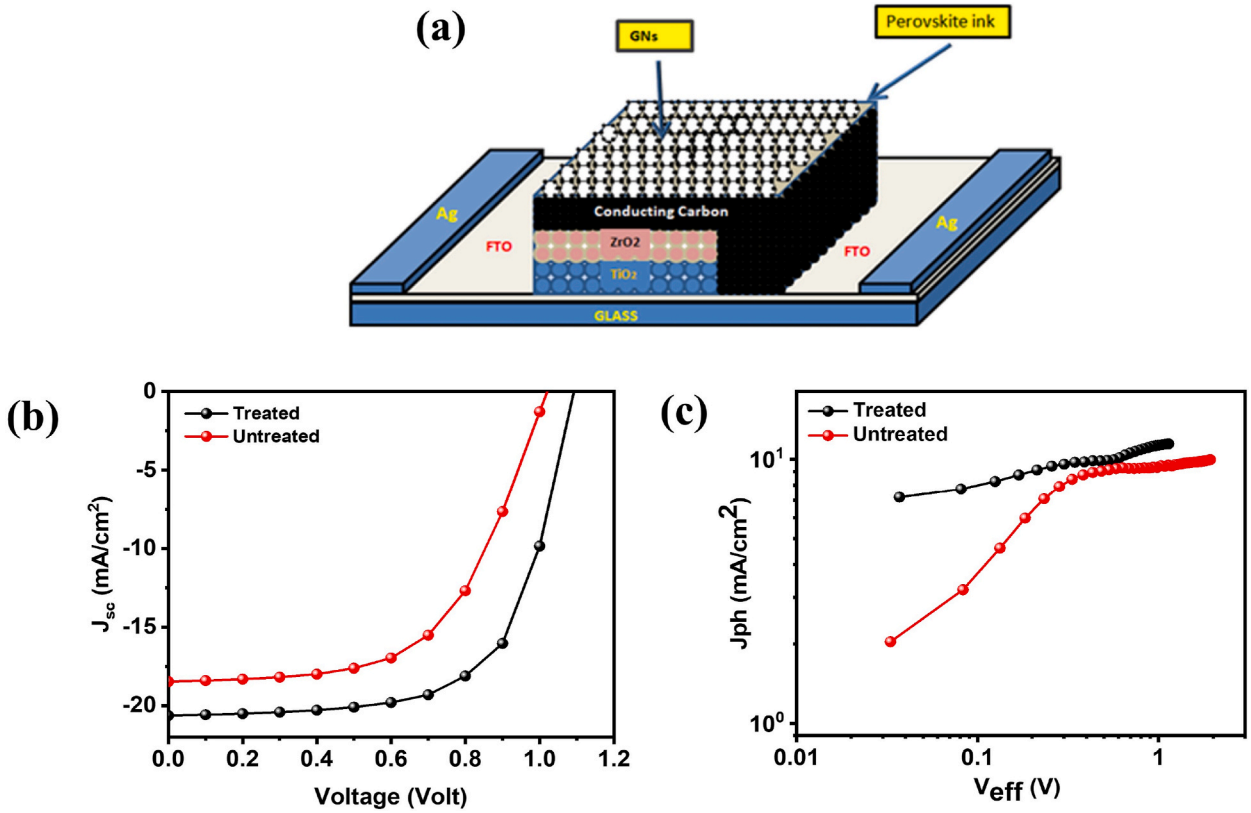

Fig. 4. (a) Device geometry of the graphene nanosheet (GN)-doped perovskite solar cell (PSC). (b) Current density–voltage (J–V) characteristics of PSC devices D1 (untreated; red line) and D2 (treated, carbon + GNs; black line). (For interpretation of the references to colour in this figure legend, the reader is referred to the Web version of this article.)

been observed from Fig. 4(c) that the treated device has a high value of diffusion current as compared to an unexposed device. The photocurrent analysis also shows that current improvement is due to better charge transport and improved interface contact between carbon electrode and perovskite active layer. The higher value of photocurrent saturation in graphene-added devices suggested a larger diffusion current and told the reason for the excellent performance in the graphene-added PSCs. The enhanced parameters of the PSCs are also associated with the high capacitance of the GNs because of their large surface area. A previous study has demonstrated that a higher capacitance of the carbon electrode results in a higher charge storage capacity and a lower charge recombination rate, increasing the efficiency and stability of PSCs [33]. The higher capacitance also improves the overall photovoltaic performance of the device by enabling more efficient charge separation and transportation. Therefore, to understand the capacitance properties, the energy storage capability of GNs was analysed by fabricating symmetrical supercapacitor devices using graphite electrodes. The GNs synthesised from waste cardboard were used as active electrode materials for graphite-based electrodes. Furthermore, 1 M H_3PO_4 was used as the electrolyte. The CV curves of the fabricated device exhibited a leaf-like shape, which deviated slightly from the standard rectangular curves (Fig. 5). The specific capacitance (C_s) was calculated from the CV curve using the following equation:

$$Cs = \int \frac{\Delta I}{2\ mk\Delta V}\ dV \tag{1}$$

Where ΔI ($I_a - I_c$) is half the integration value of the CV curve, and I_a and I_c denote the anodic and cathodic currents, respectively. Further, k represents the scan rate (mV/s), m represents the active material's mass (g), and the potential window is denoted by ΔV (V).

The GCD measurements were obtained based on the current densities of 0.5, 1, 2, and 5 A/g in the voltage range of 0–1 V. Fig. 6(a) illustrates the GCD curves of the GN-based supercapacitor device, which are nearly triangular. Therefore, the devices exhibit the fundamental characteristics of supercapacitors, whereas their reversible charging and discharging properties confirm the ideal characteristics of the electric double-layer capacitor (EDLC). The value of C_s can be obtained from the GCD curves as follows:

$$C_s = \frac{I \times \Delta t}{m \times \Delta V} \tag{2}$$

Where I represent the current (A); Δt denotes the discharging time (s); m indicates the mass loaded on the electrodes (g); and ΔV V represents the potential window used for testing. The value of C_s obtained from the CV analysis (Table 2) was approximately equal to

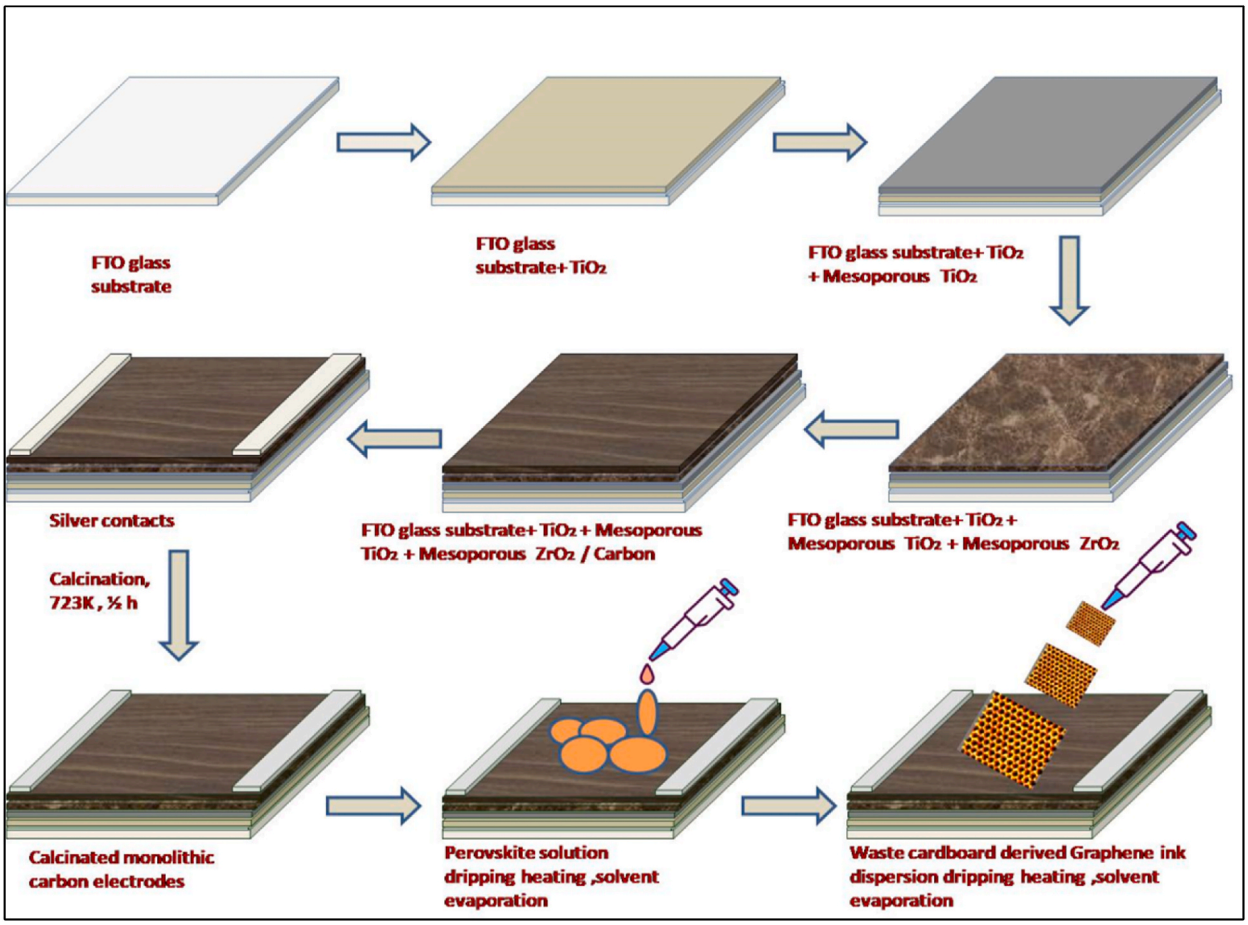

Scheme 2. Fabrication process of the graphene nanosheets (GNs) doped with carbon perovskite solar cells (PSCs).

Table 1
Various device parameters of standard PSCs and GN-based PSCs.

Device	J_{sc} (mA/cm^2)	V_{oc} (V)	Fill factor (%)	PCE (%)
Untreated	21.05	1.02	60.04	13.98
Treated	22.51	1.09	64.28	15.80

that measured using the GCD curve. However, the value of C_s tended to decrease at high current densities owing to the low diffusion rate and migration of ions between the interface of the electrode and separator. Table 3 lists the values of C_s at different current densities, including 0.5, 1, 2, and 5 A/g; the highest value is indicated in bold.

We performed EIS to investigate the material's internal resistance and analyse the GNs' capacitance. The EIS measurements were obtained using a sinusoidal signal of 10 mV in the frequency range of 10 mHz–1 MHz. Fig. 6(b) depicts the Nyquist plot obtained from the EIS data considering the actual impedance (Z) and imaginary impedance (Z'') of the fabricated device. An ideal Nyquist plot should depict a semicircle with a straight line at an angle of 90°, where the semicircle represents the charge-transfer resistance (R_{ct}) between the electrode and electrolyte. However, the Nyquist plot obtained in this study exhibited a significant deviation from the standard Nyquist plot for EDLC because only a curved line was observed in the low-frequency region; this may be attributed to the low faradaic resistance within the electrolyte. All the components were fitted into a circuit using Autolab NOVA 2.0 software, shown in Fig. 6(c), where W denotes the Warburg resistance that arose due to the straight line at 45° to the real axis. The circuit fitting reflects the value of R_s equivalent to 0.9 Ω, indicating less resistance in the electrolytic solution. The capacitance was determined using Equation (3) from the EIS data as follows:

$$C_s = -\frac{1}{2\pi f Z''} \tag{3}$$

Where f represents the lowest frequency, and Z'' denotes the imaginary impedance. Notable depression in the capacitance values

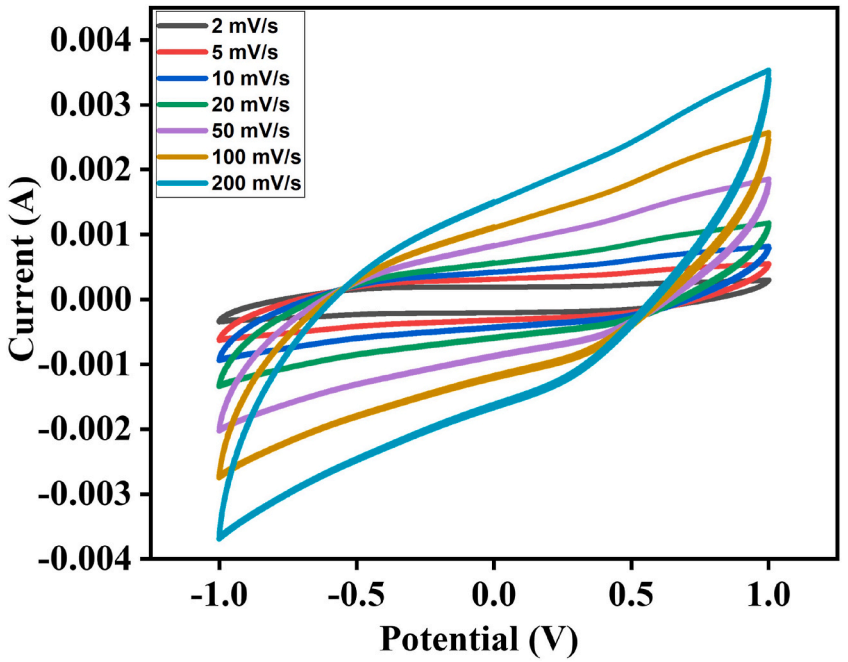

Fig. 5. Cyclic voltammetry (CV) plots of the supercapacitor devices fabricated using graphene nanosheets (GNs) at numerous scan rates.

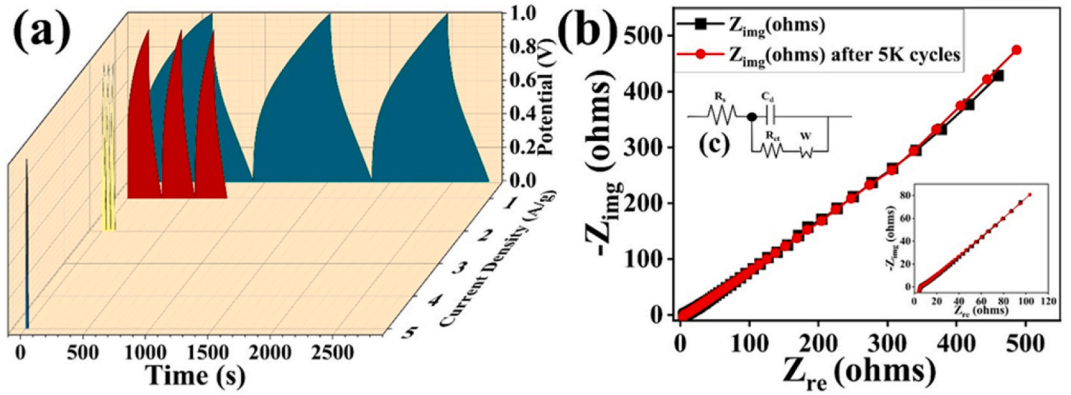

Fig. 6. (a) Galvanostatic charge–discharge (GCD) plots at different current densities of the graphene nanosheet (GN)-based supercapacitor device. (b) Electrochemical impedance spectroscopy (EIS) spectra of the GN-based supercapacitor device in the frequency range of 1 MHz–1 mHz. (c) Fitted Equivalent Circuit corresponding to the EIS data.

Table 2
Specific capacitance values of the supercapacitors at various scan rates based on the CV curve.

Scan rate (mV/s)	2	5	10	20	50	100	200
C_s (F/g)	**167.5**	107.0	72.0	48.3	28.3	18.8	12.6

Table 3
The specific capacitance of the supercapacitor device at various current densities is calculated using the GCD curves.

Current density (A/g)	0.5	1	2	5
C_s (F/g)	**166**	106	31	16

obtained using the EIS data was observed after the 5000 charge-discharge cycles. Table 4 lists the values of C_s at a frequency of 1 mHz before and after 5000 charge–discharge cycles.

The energy density (E_D) and power density (P_D) were also calculated based on the obtained capacitance of the GN-based device, as follows:

$$E_D = \frac{1}{2} C(\Delta V)^2 \tag{4}$$

$$P_D = \frac{3600 \times E_D}{\Delta t} \tag{5}$$

Where C denotes the specific capacitance; ΔV indicates the potential window of the GCD measurements; E_D represents the energy density of the GN-based SC device (Wh/kg); and Δt denotes the discharging time of the GCD curves. The GN-based SC devices exhibited an adequate E_D of 23.05 Wh/kg and a promising P_D of 256.36 W/kg.

The supercapacitors were further subjected to cyclic stability tests. Fig. 7(a) depicts the cycle life in terms of percentage capacitance retention, which indicates the high stability of the device at a high current density of 5 A/g. We observed a capacitance retention of 91.6 % after 5000 cycles of charge-discharge. Fig. 7(b) illustrates the charge–discharge cycle life at a high current density of 5 A/g, revealing a capacitance of 20 F/g, which decreases to 15.5 F/g after 5000 charge–discharge cycles.

4. Cost-benefit analysis

The cost of graphene production at the industrial level depends on several aspects such as (1) raw materials cost, (2) equipment and processing cost, (3) energy consumption, (4) environmental considerations, (5) scale of production, (7) research and development cost, and (8) market demand and competition. Among these, the cost of raw materials is one of the major factors that affect the cost of production and, hence, directly affects the economic aspects of graphene production. Thus, in this study we are addressing all the factors ang trying to estimate the graphene cost at pilot scale. At the pilot scale, the cost of the 10 g of the graphene nanosheets through the present method is estimated to be 1 USD to 5 USD, depending upon the industrial symbiosis for the availability of the waste cardboard. This cost may further decrease depending upon the plant capacity and availability of the automation processes within the graphene manufacturing plant. On the other hand, the same amount of graphene nanosheets available within the market ranges from 100 USD to 200 USD, which shows that our strategy to synthesise graphene can dramatically reduce the price of graphene and hence can be beneficial for large-scale energy conversion and storage applications.

5. Conclusions

In this study, we successfully synthesised high-quality GNs using waste cardboard and demonstrated their application in PSCs and supercapacitors. The synthesised GNs were 4–5 nm thick and exhibited suitable surface morphologies to be applied as electrode materials in supercapacitors and PSCs. Introducing GNs into the PSC electrode enhanced the charge transport properties and the device characteristics, thereby improving the short-circuit current and PCE. Similarly, when GNs were used as the material for an active layer in supercapacitors, an excellent mass-specific capacitance of 167.5 F/g was realised at a scan rate of 2 mV/s. A similar capacitance value was obtained from the GCD analysis, confirming the synthesised GNs' efficacy for supercapacitor applications. The proposed method for synthesising GNs is cost-effective, sustainable, and eco-friendly, and the study findings confirm their application in PSCs and supercapacitors. The developed process can be a promising method for upcycling waste cardboard, paving the way for waste utilisation in energy applications.

Data availability

The data generated/analysed during the present study are available from the corresponding author upon reasonable request.

CRediT authorship contribution statement

Kuldeep K. Garg: Investigation, Conceptualization. **Sandeep Pandey:** Writing – review & editing, Writing – original draft, Methodology, Investigation, Data curation, Conceptualization. **Mayank Pathak:** Writing – review & editing, Data curation. **Chetan Prakash Sharma:** Writing – review & editing, Software, Data curation. **Amit Kumar:** Formal analysis, Data curation. **Lata Pandey:** Writing – review & editing, Formal analysis. **Christopher J. Arnusch:** Formal analysis, Data curation. **Nanda Gopal Sahoo:**

Table 4
Specific capacitance values of the supercapacitor devices were calculated using data from EIS spectra.

	Z_{img}	C_s
Before 5000 cycles	428.69	74.3
After 5000 cycles	474.5	67.0

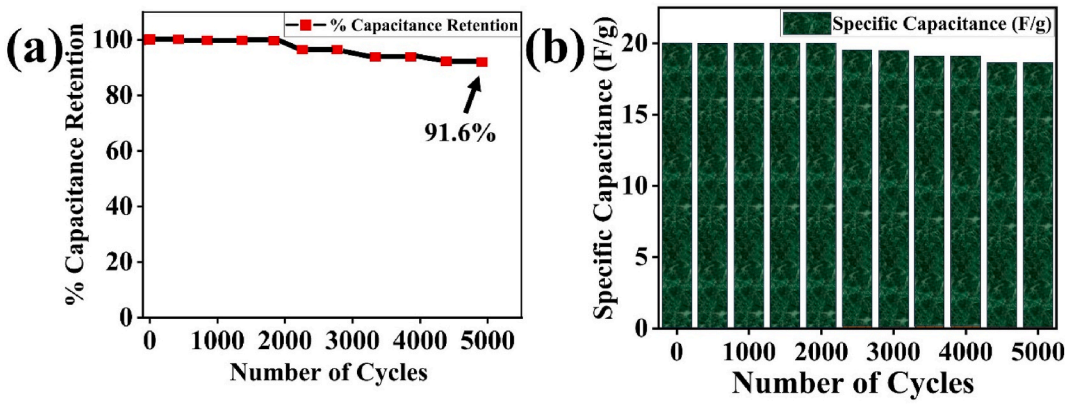

Fig. 7. (a) Cyclic stability in percentage capacitance retention at a current density of 5 A/g. (b) Cyclic stability concerning the specific capacitance (C_s).

Supervision, Resources, Funding acquisition. **S.K. Dhawan:** Formal analysis. **Man-Jong Lee:** Supervision, Resources, Funding acquisition, Data curation. **Rajiv K. Singh:** Supervision, Investigation, Funding acquisition, Formal analysis.

Declaration of competing interest

The authors declare that they have no known competing financial interests or personal relationships that could have appeared to influence the work reported in this paper.

Acknowledgement

The authors thank the Director of CSIR-National Physical Laboratory, Dr. K. S. Krishnan Marg, New Delhi. K. K. G. is thankful to the University Grants Commission, New Delhi, India, for the award of the Senior Research Fellowship. M. P. is grateful for the financial support from the DST INSPIRE division (Ref. No. IF180347). R.K.S. acknowledges DST SERD (2019) for providing financial support. M.-J. L is supported by the Basic Science Research Program through the National Research Foundation of Korea (NRF), funded by the Ministry of Education (2022R1F1A1073950) and Academic Research Grant (2023-A019-0268) by Konkuk University, Seoul, Republic of Korea.

References

[1] K.K. Garg, S. Pandey, A. Kumar, A. Rana, N. Gopal, R.K. Singh, Results in Materials Graphene nanosheets derived from waste plastic for cost-effective thermoelectric applications, Results in Materials 13 (January) (2022) 100260, https://doi.org/10.1016/j.rinma.2022.100260.
[2] Z. Sun, M. Zheng, H. Hu, H. Dong, Y. Liang, Y. Xiao, From biomass wastes to vertically aligned graphene nanosheet arrays : a catalyst-free synthetic strategy towards high-quality graphene for electrochemical energy storage, Chem. Eng. J. 336 (September 2017) (2018) 550–561, https://doi.org/10.1016/j.cej.2017.12.019.
[3] M.Z. Iqbal, A. Rehman, Recent progress in graphene incorporated solar cell devices, Sol. Energy 169 (May) (2018) 634–647, https://doi.org/10.1016/j.solener.2018.04.041.
[4] J.R. Miller, P. Simon, Electrochemical capacitors for energy management, Science 321 (August) (2008) 651–653.
[5] J. Libich, J. Maca, J. Vondrak, O. Cech, M. Sedlarikova, Supercapacitors : properties and applications, J. Energy Storage 17 (March) (2018) 224–227, https://doi.org/10.1016/j.est.2018.03.012.
[6] Q. Jin, J. Park, N. Ji, M. Khandelwal, W. Kim, Applied Surface Science Ultrafast supercapacitors based on boron-doped Ketjen black and aqueous electrolytes, Appl. Surf. Sci. 600 (July) (2022) 154181, https://doi.org/10.1016/j.apsusc.2022.154181.
[7] M. Khandelwal, C. Van Tran, J. Lee, J. Bin, Nitrogen and boron co-doped densified laser-induced graphene for supercapacitor applications, Chem. Eng. J. 428 (May 2021) (2022) 131119, https://doi.org/10.1016/j.cej.2021.131119.
[8] D. Wang, J. Nai, L. Xu, T. Sun, A Potassium formate activation strategy for the synthesis of ultrathin graphene-like porous carbon nanosheets for advanced supercapacitor applications, ACS Sustain. Chem. Eng. (2019), https://doi.org/10.1021/acssuschemeng.9b04209.
[9] S. Biswas, L.T. Drzal, Multilayered nano-architecture of variable sized graphene nanosheets for enhanced supercapacitor electrode performance, ACS Appl. Mater. Interfaces 2 (8) (2010) 2293–2300, https://doi.org/10.1021/am100343a.
[10] S. Pandey, M. Karakoti, S. Dhali, N. Karki, B. SanthiBhushan, C. Tewari, S. Rana, A. Srivastava, A.B. Melkani, N.G. Sahoo, Bulk synthesis of graphene nanosheets from plastic waste: an invincible method of solid waste management for better tomorrow, Waste Manag. 88 (2019) 48–55, https://doi.org/10.1016/j.wasman.2019.03.023.
[11] S. Pandey, M. Karakoti, K. Surana, P.S. Dhapola, B. SanthiBhushan, S. Ganguly, P.K. Singh, A. Abbas, A. Srivastava, N.G. Sahoo, Graphene nanosheets derived from plastic waste for the application of DSSCs and supercapacitors, Sci. Rep. 11 (1) (2021) 1–17, https://doi.org/10.1038/s41598-021-83483-8.
[12] S. Pandey, M. Karakoti, D. Bhardwaj, G. Tatrari, R. Sharma, L. Pandey, M.-J. Lee, N.G. Sahoo, Recent advances in carbon-based materials for high-performance perovskite solar cells: gaps, challenges and fulfillment, Nanoscale Adv. 5 (6) (2023) 1492–1526, https://doi.org/10.1039/d3na00005b.
[13] M.A. Al-Hamyd, A.S. Al-Asadi, M.F. Al-Mudhaffer, Preparation and characterization of zinc–aluminium layered doubled hydroxide/graphene nanosheet composite for supercapacitor electrode, Phys. E Low-dimens. Syst. Nanostruct. 136 (October 2021) (2022) 115005, https://doi.org/10.1016/j.physe.2021.115005.
[14] A.I. Habeeb, A.S. Al-Asadi, Fabrication of hybrid graphene nanosheets/Vanadium(V) oxide nanoparticles composite electrodes for supercapacitor application, Solid State Commun. 360 (July 2022) (2023) 115024, https://doi.org/10.1016/j.ssc.2022.115024.

[15] R. Kumar, S. Sahoo, E. Joanni, R.K. Singh, R.M. Yadav, Graphene-metal oxide hybrid materials with 2D and 3D morphologies for advanced supercapacitor electrodes: status, challenges and prospects, Materials Today Nano 24 (August) (2023) 100399, https://doi.org/10.1016/j.mtnano.2023.100399.
[16] K. Sun, S. Cui, X. Gao, X. Liu, T. Lu, H. Wei, H. Peng, G. Ma, Graphene oxide assisted triple network hydrogel electrolyte with high mechanical and temperature stability for self-healing supercapacitor, J. Energy Storage 61 (February) (2023) 106658, https://doi.org/10.1016/j.est.2023.106658.
[17] S.M. Youssry, M.A. Elkodous, R. Kumar, G. Kawamura, W.K. Tan, A. Matsuda, Thermal-assisted synthesis of reduced graphene oxide-embedded Ni nanoparticles as high-performance electrode material for supercapacitor, Electrochim. Acta 463 (March) (2023) 142814, https://doi.org/10.1016/j.electacta.2023.142814.
[18] M.J. Allen, V.C. Tung, R.B. Kaner, Honeycomb carbon : a review of graphene, Chemical Reviewscal Reviews (2010) 132–145.
[19] M. Yi, Z. Shen, A review on mechanical exfoliation for the scalable production of graphene, J. Mater. Chem. A (2015) 11700–11715, https://doi.org/10.1039/c5ta00252d.
[20] L. Lin, Synthesis challenges for graphene industry, Nat. Mater. 18 (June) (2019).
[21] G. Ruan, Z. Sun, Z. Peng, J.M. Tour, Growth of graphene from food , insects , and waste, ACS Nano 9 (2011) 7601–7607.
[22] L. Ghorbel, T. Rouissi, S.K. Brar, D. López-gonzález, A.A. Ramirez, S. Godbout, Value-added performance of processed cardboard and farm breeding compost by pyrolysis, Waste Manag. 38 (2015) 164–173, https://doi.org/10.1016/j.wasman.2015.01.009.
[23] X. Wang, F. Sotoudehniakarani, Z. Yu, J.J. Morrell, J. Cappellazzi, A.G. Mcdonald, Evaluation of corrugated cardboard biochar as reinforcing fi ber on properties , biodegradability and weatherability of wood-plastic composites, Polym. Degrad. Stabil. 168 (2019) 108955, https://doi.org/10.1016/j.polymdegradstab.2019.108955.
[24] N.H. Barbhuiya, A. Kumar, A. Singh, M.K. Chandel, C.J. Arnusch, J.M. Tour, S.P. Singh, The future of flash graphene for the sustainable management of solid waste, ACS Nano 15 (10) (2021) 15461–15470, https://doi.org/10.1021/acsnano.1c07571.
[25] D. Lee, J. Lu, J. Chang, Bioresource Technology Pyrolysis synergy of municipal solid waste (MSW): a review, Bioresour. Technol. 318 (June) (2020) 123912, https://doi.org/10.1016/j.biortech.2020.123912.
[26] S. Kaza, L.P.B.T. Yao, F.V. W, What a Waste 2.0: A Global Snapshot of Solid Waste Management in 2050, World Bank Group. World Bank Group, Washington, DC, 2018.
[27] B. Delgado, D.L. González, S. Godbout, R. Lagacé, A. Giroir-fendler, A.A. Ramirez, Science of the Total Environment A study of torre fi ed cardboard characterization and applications : composition , oxidation kinetics and methane adsorption, Sci. Total Environ. 593–594 (2017) 406–417, https://doi.org/10.1016/j.scitotenv.2017.03.119.
[28] P. Randolph, R.R. Bansode, O.A. Hassan, D. Rehrah, R. Ravella, M.R. Reddy, D.W. Watts, J.M. Novak, M. Ahmedna, Effect of biochars produced from solid organic municipal waste on soil quality parameters, J. Environ. Manag. 192 (2017) 271–280, https://doi.org/10.1016/j.jenvman.2017.01.061.
[29] S. Pandey, A. Kumar, M. Karakoti, K.K. Garg, A. Rana, G. Tatrari, B.S. Bohra, P. Yadav, R.K. Singh, N.G. Sahoo, 3D graphene nanosheets from plastic waste for highly efficient HTM free perovskite solar cells, Nanoscale Adv. 3 (16) (2021) 4726–4738, https://doi.org/10.1039/d1na00183c.
[30] T. Li, R. Ma, X. Xu, S. Sun, J. Lin, Microwave-induced preparation of porous graphene nanosheets derived from biomass for supercapacitors, Microporous Mesoporous Mater. 324 (June) (2021) 111277, https://doi.org/10.1016/j.micromeso.2021.111277.
[31] K. Rathinam, S.P. Singh, Y. Li, R. Kasher, J.M. Tour, C.J. Arnusch, Polyimide derived laser-induced graphene as adsorbent for cationic and anionic dyes, Carbon 124 (2) (2017) 515–524, https://doi.org/10.1016/j.carbon.2017.08.079.
[32] N.H. Barbhuiya, A. Kumar, A. Singh, M.K. Chandel, C.J. Arnusch, J.M. Tour, S.P. Singh, Sustainable management of solid waste, ACS Nano (2021), https://doi.org/10.1021/acsnano.1c07571.
[33] T. Berestok, C. Diestel, N. Ortlieb, J. Buettner, J. Matthews, P.S.C. Schulze, J.C. Goldschmidt, S.W. Glunz, A. Fischer, High-efficiency monolithic photosupercapacitors: smart integration of a perovskite solar cell with a mesoporous carbon double-layer capacitor, Sol. RRL 5 (11) (2021) 1–13, https://doi.org/10.1002/solr.202100662.